Supercritical water hydrolysis combined with silver mesoporous zeolite catalysts for the hydrolysis of cellulose into glucose

S. G. Aspromonte[a], A. Romero[b], A. V. Boix[a], E. Alonso[b,*]

[a] Instituto de Investigaciones en Catálisis y Petroquímica – INCAPE (FIQ, UNL-CONICET) - Santiago del Estero 2829, 3000, Santa Fe, Argentina.

[b] High Pressure Processes Group –Chemical Engineering and Environmental Technology Dpt., Universidad de Valladolid, c/Prado de la Magdalena 5, 47011, Valladolid, Spain.

Corresponding author. Tel: +34 983 423 175

[*]E-mail address: ealonso@iq.uva.es

SUBMITTED TO CELLULOSE

Graphical Abstract

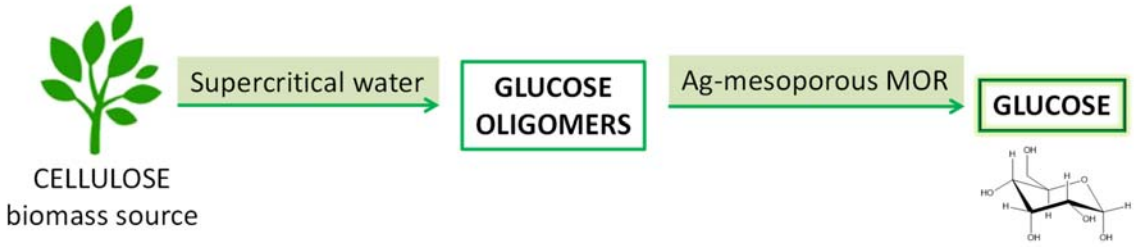

Highlights

1. Crystalline cellulose is hydrolyzed into glucose with a yield of 63.8%
2. The Ag(I) ions exchanged allowed the hydrolysis of cellulose
3. The incorporation of silver produces a redistribution of acid sites
4. Al(III) species which are octahedrically coordinated were detected

Abstract

The hydrolysis of cellulose into glucose is a critical step for the conversion of lignocellulosic biomass into fuels and chemical products. The combination of supercritical water hydrolysis in ultrafast reactors, with the subsequent hydrolysis of the cello-oligosaccharides on silver-exchanged mesoporous mordenite zeolite, offers the possibility of a clear enhancement in the conversion of cellulose and in glucose formation. Complete dissolution of cellulose is achieved in the supercritical step and 81.8% of formed oligosaccharides are hydrolyzed in the catalytic step, with a yield into glucose of 77.0 %. A fraction of Al is octahedrally coordinated, indicating a distribution of acid sites after the silver exchange. A deactivation of the catalyst between the first and third reaction cycle is observed, with a reduction in hydrolyzed carbon from 81.8% up to 45.6%. However, the selectivity to glucose only varies from 94.1 to 81.8%. Afterwards, the activity remains constant up to the fifth cycle. The presence of Ag(0) particles, together with the formation of coke, are responsible for the partial blockage of the pores of the support and loss of catalytic activity.

Keywords: hydrolysis of cellulose; mordenite; glucose; biomass; silver; mesoporous zeolite

1. Introduction

In the last years, there is a general tendency towards a society supported by the bioeconomy and in the use of renewable resources.

In this context, the hydrolysis of cellulose to glucose is an important process and remains a challenge for the conversion of lignocellulosic biomass to fuels and chemicals. Supercritical water (SCW) in ultrafast reactors with hydrolysis times of milliseconds has demonstrated to possess good ability to partially depolymerize cellulose without further degradation of sugars (Cantero 2013, 2015). Although under such conditions more than 99 % of the cellulose is solubilized, the presence of oligomers remains high (> 60 % C) (Cantero 2015). A possible approach to solve this problem is to complete the hydrolysis of cellulose into glucose by solid acid catalysts, representing an alternative to the enzymatic hydrolysis (Chheda 2007) or to the use of mineral acids (Chimentao 2014). Various solid acids including sulfonated carbons, niobic acid, sulfonated resins, (Suganuma 2008, Yamaguchi 2009), acid resins, metal oxides, H-form zeolites, heteropoly acids, functionalized silicas, supported metals, immobilized ionic liquids, carbonaceous acids and magnetic acids (Hu 2015), (Inumaru 2007), MoO_3-ZrO_2, tungstate zirconium phosphate, zirconium phosphate, lanthanum phosphate niobium and some other materials (Morales-de la Rosa 2018) have been studied to catalyze the cellulose hydrolysis. Conceptually, solid acids having high specific surface areas, pore size/volume and strong acid sites are prone to exhibit better performances in the reaction. Among these solid acids, zeolites are one of the promising catalysts due to their crystalline structure, uniform pore size, high surface area, flexible framework and tunable acidity.

Nevertheless, zeolites defining accessible pores of effective dimensions and allowing the access and escape of many small-sized reagents but excluding the processing of bulky

72 molecules. Furthermore, these porous networks impose diffusional limitations on the reacting
73 molecules, reducing the mass transport to and away from the reactive sites in the pore system
74 and opening time windows for unwanted secondary reactions and coke formation (Zapata
75 2012). Cho et. al (2014) reported that the glucose diffusion inside the 5.1-5.6 Å pores of the
76 ZSM5 was significantly hindered compared to β zeolite (5.6-6.7 Å) and carbohydrates can
77 only react with active sites located on the outer pore rims. As it can be observed, until now,
78 there are very few works that report catalysts based on transition metals for the hydrolysis of
79 cellulose into sugars and, up to our knowledge, there is not any work using mesoporous
80 zeolites.
81 Hence, the aim of the present work is to maximize the glucose yield from microcrystalline
82 cellulose using heterogeneous catalysts to complete the hydrolysis of oligomers derived from
83 supercritical water hydrolysis in ultrafast reactors. For this purpose, the behaviour of Ag-
84 based catalysts exchanged in mesoporous Na-mordenite was studied. This performance is
85 compared to the commercial acid zeolite (HMOR, Si/Al=10) in an inert and reducing
86 atmosphere.
87 In addition, to achieve a global understanding of the observed catalytic behaviour several
88 physicochemical techniques were applied, such as adsorption/desorption isotherms of N_2 and
89 measurements of X-ray photoelectron (XPS) and solid-state NMR spectroscopies,
90 programmed-temperature reduction (TPR) and programmed-desorption temperature of
91 ammonia (TPD-NH_3).
92

93 # 2. Materials and Methods

94 ## 2.1 Supports and Catalysts

Commercial microporous zeolites were used, Na-mordenite (CBV 10A Zeolyst International, Si/Al = 6.5) labeled MOR and NH_4-mordenite (CBV 21A Zeolyst International, Si/Al = 10). From the latter, the protonated form denoted H-MOR was obtained by calcination in air flow at 550 °C for 8 hours.

2.1.1 Synthesis of mesoporous zeolite (m-MOR)

The m-MOR mesoporous support was synthesized using the CTMABr (bromide hexadecyl trimethyl ammonium chloride) surfactant as directing agent and a commercial Na-mordenite zeolite as a source of Si and Al. For that, 3 g of CTMABr were dissolved in water at room temperature and with continuous stirring. Absolute ethanol was added as solvent and a solution of NH_4OH 29 wt. %. Subsequently, the mordenite was added and stirred for 18 h at 25 °C. The molar composition used for the synthesis is 0.024 NaMOR:0.3 CTMABr:11 NH_3:144 H_2O:58 EtOH.

The final solid was obtained by vacuum filtration, and several washes were performed to achieve neutral pH. Then, the samples were dried in an oven for 12 h at 80 °C and calcined in air at 1 °C · min^{-1} to 550 °C.

2.1.2 Incorporation of silver (Ag/m-MOR)

Silver was incorporated by a conventional ion exchange between the calcined m-MOR support and a solution of $AgNO_3$ (0.07 M) at room temperature for 24 hours under continuous stirring. Ion exchange is performed in the absence of light to avoid reduction of the species to Ag(0). Then, the samples were filtered, washed with deionized water, dried and calcined in air at a flow rate of 1 °C · min^{-1} to 550 °C. The silver content was determined by Plasma Spectroscopy (ICP-OES). The Ag/m-MOR catalyst has 9.6 wt. % of silver.

2.2 Catalyst characterization

The catalysts were characterized by nitrogen adsorption/desorption, small angle X-ray scattering (SAXS), X-ray diffraction (XRD), temperature-programmed reduction (TPR) or desorption of ammonia (TPD-NH_3), X-ray photoelectron (XPS) and solid-state NMR spectroscopies.

Specific surface area, pore size distribution and total volume were determined from N_2 adsorption/desorption isotherms obtained at -196 °C using a Quantachrome Autosorb instrument. Previously, the samples were outgassed at 350 °C for 6 h (10^{-4} torr). The specific surface area was calculated using the standard BET method (Brunauer 1938) for N_2 adsorption data in the relative pressure adsorption range from 0.05 to 0.1. The BJH method was used for the distribution of pore size.

The X-ray diffractograms were analyzed using a Shimadzu XD-D1 instrument equipped with an X-ray tube with monochromatic CuKα radiation and Ni filter. The measurement was conducted between 5 and 85° values of 2θ, with a speed of 1 °·min^{-1}, 30 kV and 40 mA. The crystallinity was estimated from the ratio of the sum of the intensity of the prominent peaks corresponding to planes (1 1 1), (3 3 0), (1 5 0), (2 0 2) and (3 5 0) of catalysts. The maximum degree of crystallinity was taken equal to 100 % and corresponded to calcined MOR (Mignoni 2008).

SAXS patterns were collected at room temperature on a Philips X'Pert diffractometer 5000. The samples were irradiated with a beam of CuKα (λ = 1.5405622 Å) without monochromator. The measurement conditions were 40 kV and 20 mA with values of 2θ between 1 and 10°.

The XPS measurements were carried out using a multitechnique system (SPECS) equipped with a dual Mg/Al X-ray source and a hemispherical PHOIBOS 150 analyzer operating in the fixed analyzer transmission (FAT) mode. The spectra were obtained with a pass energy of 30 eV using Mg Kα X-ray source (hν = 1253.6 eV) operated at 200 W and 12 kV. The working pressure in the analyzing chamber was less than 5 x 10^{-10} kPa. The binding energy (BE) positions of Ag 3d do not identify the oxidation state of the silver species, because the characteristic states of oxidized (Ag_2O) and metallic silver (Ag (0)) are close together (within 0.5 eV) (Aspromonte 2012, 2013). Thus, the modified Auger parameter (α′) was used to characterize the chemical state of silver. This parameter is the sum of the kinetic energy (KE) of the Auger electron (Ag M_4NN) and the BE of the core-level (Ag $3d_{5/2}$) peak. The BE of core-levels Si 2p, Al 2p, Ag 3d, C 1s, O 1s and the KE in the region of the Ag M_4NN auger transitions were measured. During the processing of XPS spectra, BE values were referenced to the C 1s peak (284.6 eV) from the adventitious contamination layer. Solid-state NMR spectroscopy was performed in a Bruker equipment, model Avance II 400 and 300 MHz, probe = 7 mm, spinning rate = 4 kHz, pulse angles = p/6 with recycle delay of 60 s and p/4 with recycle delay of 2 s for the experiment of ^{29}Si and ^{27}Al, respectively.

The temperature-programmed desorption of ammonia (TPD-NH_3) was performed with 100 mg of catalyst, which was pretreated *in-situ* with He flow (30 ml·min^{-1}) at 350 °C during 1 hour. After cooling down to 100 °C, the sample was saturated with 50 cm^3·min^{-1} ammonia flow during 30 minutes. Then, He was flowed and the temperature was increased up to 150 °C, maintaining this temperature until no physically adsorbed ammonia was detected. The TPD experiment was carried out heating at 15 °C·min^{-1} in He flow from 150 to 750 °C and using a Micromeritics TPD-TPR 2900 equipment.

The temperature-programmed reduction (TPR) experiments were run with 100 mg of catalyst at a heating rate of 10 °C·min^{-1} and a H_2/Ar (5%) flow rate of 50 cm^3·min^{-1}. The used equipment was a Micromeritics with AutoChem II chemisorption analyzer.

2.3 Catalytic Performance

The catalysts were evaluated in the hydrolysis of cellulose oligomers derived from the hydrolysis of microcrystalline cellulose (Avicel® PH-101, Sigma-Aldrich) in ultrafast supercritical reactors at 400 °C, 25 MPa and 0.03 s. Details of the experimental facility are included in previous works (Cantero 2013). Under such conditions 99.9 % of the cellulose is solubilized in water (Cantero 2013) but more than 66% of solubilized carbon is still forming cello-oligosaccharides. The purpose of the subsequent catalytic step was to complete the oligosaccharide hydrolysis maximizing the glucose production in the final product. The outline of the procedure is summarized in Figure 1.

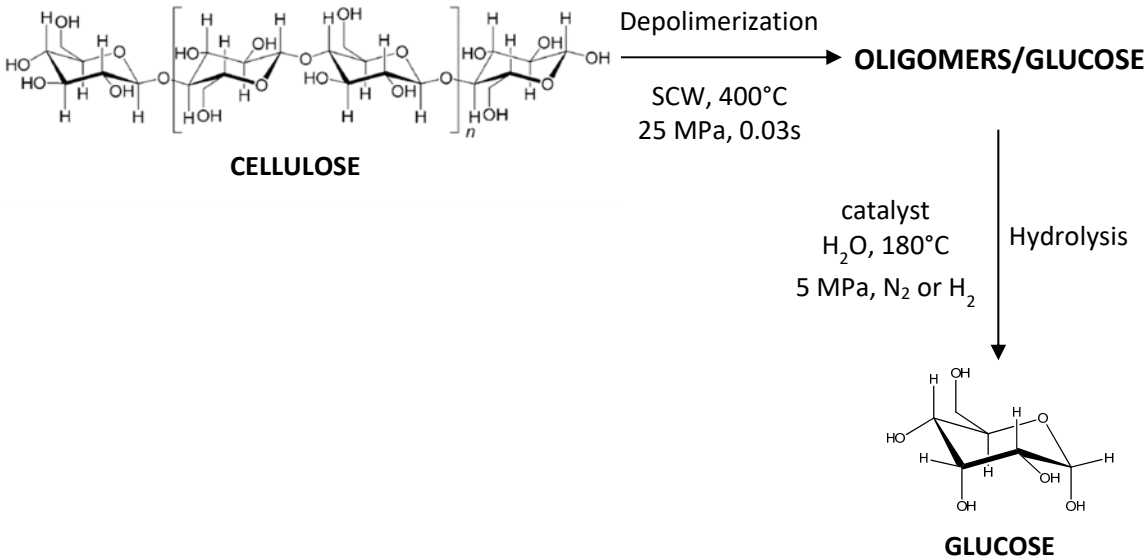

Figure 1. Scheme of the global hydrolytic process.

Catalytic tests were performed in a commercial AISI 304 stainless steel batch reactor with an internal volume of 25 ml (Berghof® BR-25). First, the catalyst was placed inside the reactor and after closing it was vented three times with nitrogen. Then, the reactor was pressurized with N_2 or H_2 up to 50 bar and heated up to the operating temperature (180 °C). Then, a volume of 20 ml of the solution obtained in the supercritical reactor was pumped at 50 °C (PU-2080 Plus, Jasco). In all the experiments, the amount of catalyst was 0.06 g of metal/g C in the feed solution. The operating time was 90 min under continuous stirring at 1400 rpm.

When the final reaction time was achieved, the reactor and its content were quenched using an ice bath to rapidly stop the reaction. After that, the product mixture was centrifuged and the supernatant solution was then filtered prior to analysis by High Performance Liquid Chromatography (HPLC). Sugars and their derivatives were determined by HPLC using a Shodex SH-1011 column at 50 °C and H_2SO_4 (0.01 N, 0.8 ml·min^{-1}) as the mobile phase and a Waters RI detector 2414, Total organic carbon (TOC) was determined using a Shimadzu TOC-VCSH analyzer.

The selectivity to D-glucose in terms of carbon was calculated for the catalytic step using equation (1):

$$S_{D-glucose}(\%) = \frac{C(D-glucose)_{out} - C(D-glucose)_{in}}{C\ hydrolyzed} \cdot 100 \qquad \text{Eq. (1)}$$

where '$C(D\text{-glucose})_{out}$' are the moles of carbon after the reaction corresponding to the D-glucose, '$C(D\text{-glucose})_{in}$' are the moles of carbon corresponding to the D-glucose in the hydrolysate obtained in the SCW step and 'C hydrolyzed' are the moles of carbon hydrolyzed in the catalytic step, and it is calculated by equation (2):

$$C\ hydrolyzed = (C_{oligomers})_{in} - (C_{oligomers})_{out} \quad \text{Eq. (2)}$$

where, '$C_{oligomers,in}$' and '$C_{oligomers,out}$' are the moles of carbon corresponding to the oligomers present before and after the catalytic reaction, respectively. '$C_{oligomers}$' is determined through a carbon balance by difference between the TOC of the sample and the carbon detected by HPLC in cellobiose, glucose, fructose, glyceraldehyde and glycoaldehyde. For this, it is assumed that the carbon remnant corresponds in its entirety to the presence of oligosaccharides, because the concentration of pyruvaldehyde was always below 3% and neither 5-HMF nor other degradation products were detected.

D-glucose yield (%) was obtained dividing moles of carbon formed in D-glucose by moles of carbon in oligomers that enter the catalytic step (Eq. (3)):

$$Y_{D-glucose}(\%) = \frac{C\ (D-glucose)_{out} - C\ (D-glucose)_{in}}{(C\ oligomers)in} \cdot 100 \quad \text{Eq. (3)}$$

and the percentage of hydrolyzed carbon in the catalytic step was determined by equation (4):

$$C_{hydrolyzed}(\%) = \frac{(C_{oligomers})_{in} - (C_{oligomers})_{out}}{(C\ oligomers)in} \cdot 100 \quad \text{Eq. (4)}$$

The selectivity to 5- (hydroxymethyl) furfural (5-HMF) was determined with equation (5):

$$S_{5-HMF}(\%) = \frac{C\ (5-HMF)}{C\ hydrolyzed} \cdot 100 \quad \text{Eq. (5)}$$

where, 'C (5-HMF)' are the moles of carbon related to 5-HMF compound.

2.4 Recycling study

The most promising Ag/m-MOR catalyst was exposed to a recycling test to study its catalytic stability. The recycling study was carried out in a similar way to the catalytic performance. First, the catalyst was separated from the products by filtration between the runs, dried at 60ºC and re-used. Five consecutive cycles were performed. The reaction products were identified and quantified by HPLC.

The nature of the Ag species formed after each reaction cycle was studied by XRD. The amount of deposited carbon during the hydrolysis reaction was determined by temperature-programmed oxidation (TPO) after each reaction cycle. The TPO experiments were carried out using a Micromeritics Autochem TM II 2920 instrument, under a gas flow of 5 % O_2 in He, and a temperature ramp of 10 ºC min^{-1}. Before the TPO experiments, catalysts were dehydrated in situ at 300 ºC in He flow.

3. Results and Discussion

3.1 Physicochemical characterization

3.1.1 Porous structure of the catalysts

Table 1 shows the quantitative values derived from the characterization of textural properties of the catalysts, i.e. BET surface area, pore volume and pore diameter, crystallinity degree and acid sites by TPD-NH_3.

Table 1. Textural and acid properties of catalysts

Catalysts	S_{BET}[(1)]	V_{micro}[(2)]	V_{meso}[(3)]	Dp[(4)]	%Crist[(5)]	Acid sites/mmol·g^{-1}		
						Total	Weak (T < 350°C)	Strong (T > 350°C)
m-MOR	532.9	0.18	0.14	4.1	65.3	0.72	0.72	-
Ag/m-MOR	425.4	0.13	0.10	3.9	42.5	1.75	0.75	1.02
Ag/m-MOR-R[(6)]	408.5	0.10	0.10	3.9	39.8	1.45	0.40	1.05

(1) Surface area BET, $m^2 \cdot g^{-1}$; (2) Micropore volume calculated by t-plot method, $cm^3 \cdot g^{-1}$; (3) Mesoporous volume calculated by BJH method, $cm^3 \cdot g^{-1}$; (4) Pore diameter, nm; (5) Crystallinity calculated using the ratio of the sum of the intensity of the five most intense peaks, (6) Ag/m-MOR-R catalyst reduced in H_2 flow at 500 °C.

The mesoporous mordenite (m-MOR) presents a type IV isotherm (not shown) according to the IUPAC nomenclature (Aspromonte 2017), which is characteristic of mesoporous materials. The surface area was 532.9 $m^2 \cdot g^{-1}$ and the micropore and mesopore volume were 0.18 and 0.14 $cm^3 \cdot g^{-1}$, respectively (Table 1). In addition, the Ag/m-MOR and Ag/m-MOR-R showed a type IV isotherms and the specific area and pore volume slightly decreased compared to the values reported for m-MOR, due to the addition of a bulky cation such as Ag. The incorporation of silver did not significantly modify the pore diameter, which would allow the voluminous oligomer molecules to reach the active centers.

In addition, the percentage of crystallinity obtained from the X-ray diffractograms (XRD) is included in Table 1. A decrease in the intensity of the major peaks was observed, indicating a loss of crystallinity in mesoporous zeolite materials from 65.3 % for m-MOR to 39.8 % for Ag/m-MOR-R. Moreover, the diffractogram did not show the signals corresponding to silver oxides or metallic species.

On the other hand, it is important to notice that the diffractograms obtained by SAXS do not show diffraction peaks in the 2θ region between 1 and 10°, which implies that the synthesized material has mesoporosity and high specific surface area, but there is no evidence of mesoporous ordering.

3.1.2 Reducibility of silver species

The properties of the active sites are related to the different species of silver present in the catalyst. Temperature-programmed reduction (TPR) helps to discerning these species. Figure 2 shows the results obtained by TPR for calcined Ag/m-MOR catalyst.

The reduction profile exhibits peaks in three temperature regions which can be attributed to different silver species. At low temperature, below 300 °C (region I), the reduction peaks could correspond to small highly dispersed particles which may be associated with Ag_xO_y species (Westermann 2012). Different peaks present in this region suggest a diverse interaction between the oxide particles and the channels of the support (Aspromonte 2012). The reduction at temperatures between 300 and 600 °C (region II) is generally attributed to Ag(I) ions at exchanged positions. Besides, there is a small fraction above 600 °C (region III) that could be assigned to Ag(I) ions located at very stable sites with high coordination, in which the cation strongly interacts with the support structure. The calculated H_2 consumption/Ag molar ratio is close to 0.5, indicating the complete reduction of Ag(I) species to their metallic state.

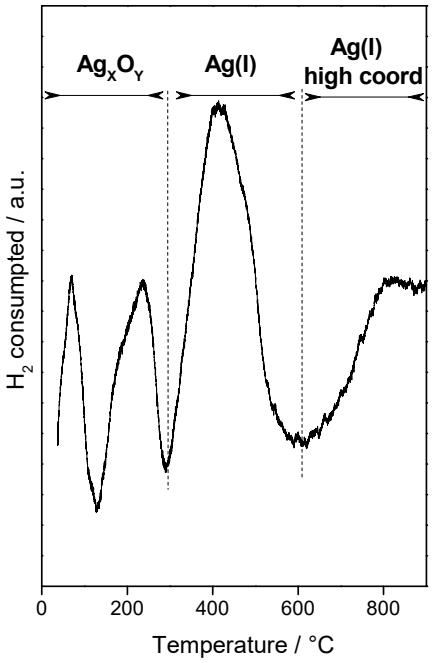

Figure 2. Results of Ag/m-MOR catalyst obtained by Temperature-Programmed Reduction (TPR).

3.1.3 XPS Surface characterization

In order to investigate the chemical state of Ag(I) exchanged species and supported nanoparticles (Ag(0) and Ag_2O), the Ag 3d photoelectron spectrum of Ag/m-MOR catalyst was measured (inlet figure in Fig. 3A).

In the literature, it is reported that the binding energy difference between Ag(0) and Ag(I) corresponding to Ag_2O is only 0.3 eV, making difficult to determine the oxidation state of silver. As a consequence of this, the M_4NN transition of the Auger region was measured (Figure 3B). By means of the calculation of the modified Auger parameter (α'), remarkable differences could be obtained. In this sense, Waterhouse et al. (2007), reported values of α' equal to 726.3 eV for Ag(0) and 724.5 eV for Ag_2O species. In previous articles of the group, a modified auger parameter values close to 722 eV were reported, corresponding to Ag (I) ions located in exchange positions within the mordenite (Westermann 2012).

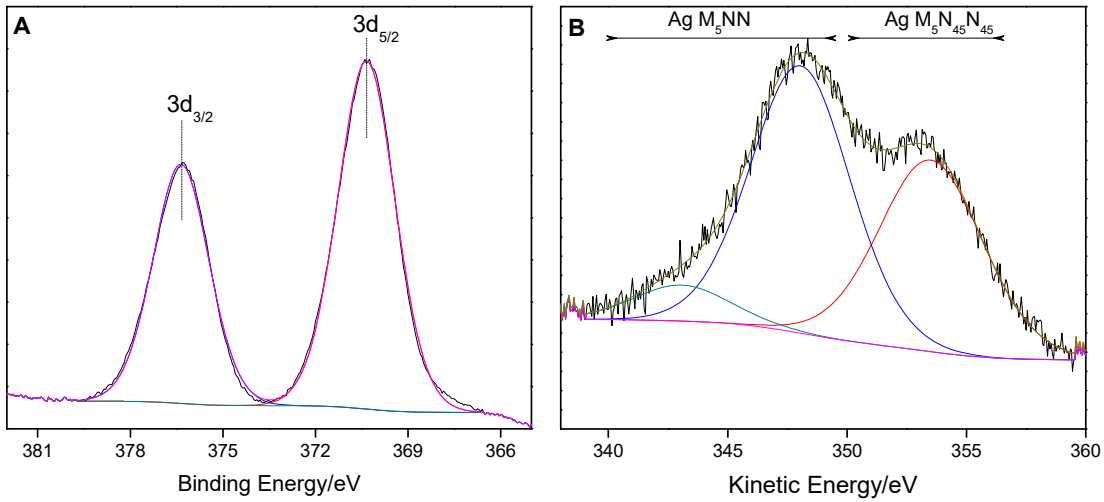

Figure 3. XPS spectrum of Ag/m-MOR catalysts, (A) Ag 3d and (B) Ag M_4NN region.

323 The modified Auger parameter for the Ag/m-MOR catalyst was calculated and it was 722.6
324 eV, which indicates the presence of Ag(I) ions in interaction with the mesoporous zeolite
325 structure, in concordance with the TPR results.
326 On the other hand, the binding energy of the Al 2p region was studied to identify the oxidation
327 state of the aluminum. In general, the mordenite sample has a single peak at 74.1 eV with
328 fwhm = 1.9 eV, which is characteristic of the tetrahedral aluminum atoms of the zeolites,
329 such as AlO_4 groups (Boix 2008).
330 After modifying the original zeolite with the generation of mesopores and the addition of 9.6
331 wt. % of silver, the binding energy of the main peak is shifted towards higher BE values. In
332 the open literature, there are numerous studies that report BE values close to 74.5 eV for
333 octahedral aluminum within the Al_2O_3 oxide (Amama 2010). The m-MOR and Ag/m-MOR
334 catalysts have BE values of 74.2 and 74.5 eV, respectively. In the same way, an increase of
335 the full width at half maximum (fwhm) to values of 2.3 and 2.5 is observed for the m-MOR
336 and Ag/m-MOR catalysts, respectively. This would indicate a modification in the chemical
337 environment of the aluminum species, probably due to the presence of surface octahedral
338 aluminum.
339
340 *3.1.4 Solid state NMR determination of mesoporous zeolite topological structure*
341 ^{29}Si (MAS) and ^{27}Al (MAS) NMR measurements were performed to reach a full
342 understanding of the system after the modification of zeolite and incorporation of silver. The
343 basic structural units of zeolitic materials based on silicates and aluminosilicates are TO_4
344 tetrahedral with silicon atoms at the central T-positions. In the second coordination sphere of
345 these T-atoms, aluminum can be incorporated into the framework. Depending on the amount
346 of aluminum atoms, which are incorporated, the tetrahedrally coordinated silicon atoms (Q^4)

in aluminosilicates may be characterized by up to five different environments denoted as Si(nAl) with n = 0, 1, 2, 3 and 4 (Stepanov 2016). Typically, the ^{29}Si MAS NMR signal of Si(0Al) species occur at ca. -110 ppm (referenced to tetramethylsilane) (Meynen 2009). Figures 4A and 4B present the results of ^{29}Si MAS NMR and ^{27}Al MAS NMR spectroscopy, respectively. The calcined MOR and m-MOR catalysts have the peaks corresponding to Q^3 and Q^4 very well defined. However, after the exchange of silver with the structure, the peak assigned to Q^2 is resolved with a contribution of 5 %. These results imply that the silicon environment after silver exchange was slightly modified.

On the other hand, according to the Loewenstein's rule, the formation of Al-O-Al bonds in aluminosilicates is forbidden, and only Al(4Si) species can exist in the corresponding frameworks (Abdelrasoul 2017). Therefore, ^{27}Al MAS NMR spectra of hydrated aluminosilicates consist, in general, of only one signal of tetrahedrally coordinated framework aluminum (Al^{tet}) at chemical shifts of ca. 50-60 ppm (referenced to a 0.1 M aqueous solution of $Al(NO_3)_3$ in D_2O). Octahedrally coordinated aluminum species (Al^{oct}) in hydrated aluminosilicates, which can be due to extra-framework aluminum compounds, induce ^{27}Al MAS NMR signals at ca. 0 ppm. Figure 4B shows the ^{27}Al MAS NMR results of MOR (spectrum a), m-MOR (spectrum b) and Ag/m-MOR (spectrum c) catalysts. All the samples present a narrow signal at 53 ppm due to tetrahedrally coordinated framework aluminum. In the case of the modified mordenite catalysts with mesoporous and/or silver species, the spectra show an additional peak at ca. 0 ppm due to octahedrally coordinated aluminum species. Specifically, after incorporating the 9.6 wt. % Ag in the structure, a broad background signal at ca. 0 ppm is observed, indicating the presence of Al_2O_3 or oxide hydrates (Meynen 2009).

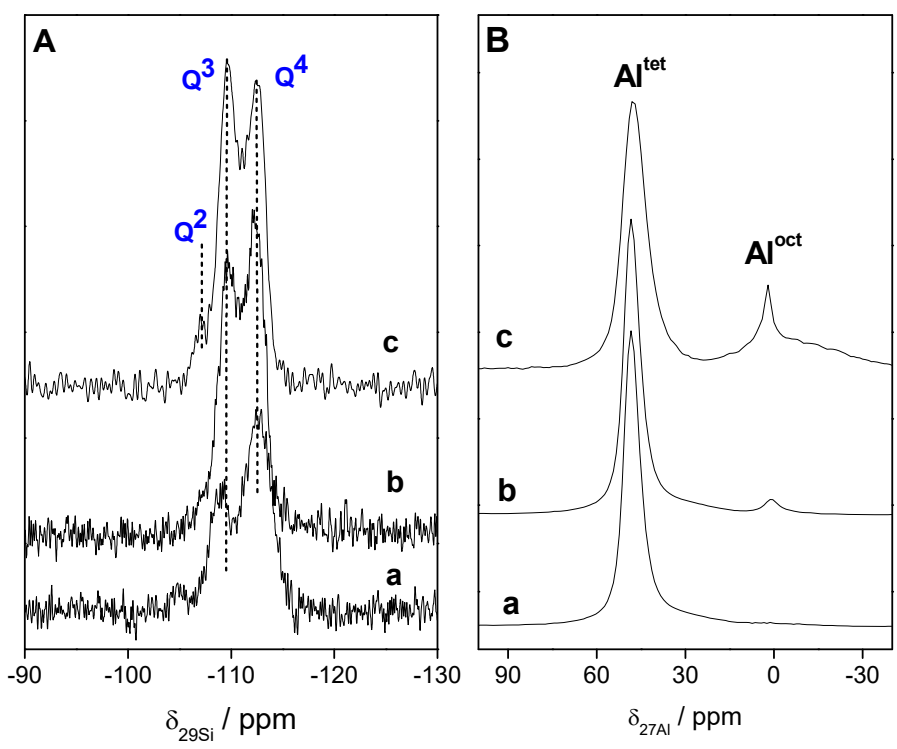

Figure 4. (A) ^{29}Si and (B) ^{27}Al MAS NMR spectra of (a) MOR, (b) m-MOR and (c) Ag/m-MOR catalysts.

In this context, Gardner et. al (2015) claimed that the presence of NaCl enhances the hydrolysis of Si-O-Al bridges and the release of Al(III) species that catalyze the isomerization of glucose to fructose. Ravenelle et. al (2015) studied the behaviour of Pt-Al_2O_3 in the hydrolysis of cellulose. They propose that the Al(III) cations [$Al(OH)_2^+$, AlO^+] interacts with OH^- ions, shifting the dissociation equilibrium of water and increasing the concentration of protons and, thus the hydrolysis activity.

It is known that all Al (III) species promote the acid-catalyzed hydrolysis of cellulose and the isomerization of glucose to fructose through Lewis acid-catalyzed intramolecular hydride shift (Saha 2014).

It is important to notice that according to the XRD results, it was observed that the crystalline fraction of the catalysts was modified in the generation of mesopores and the incorporation

396 of silver. This could be linked to the Si-O-Al bonds involved in extra-structural species and/or
397 defective sites that suffers a hydrolytic attack, resulting in the leaching of the aluminum to
398 the synthesis medium. In addition, by means of XPS and ^{27}Al MAS NMR spectroscopies, it
399 is shown that a fraction of Al is octahedrally coordinated, most likely as Al(III) ions.
400 The cellulose is formed by the binding of β-glucopyranose molecules via β-1,4-glucosidic
401 bonds. Cellulose chains are coupled together in bundles hydrogen bridges. Therefore, in the
402 first step, due to the low solubility, hydrolysis of cellulose in water can only proceed on the
403 outer surface of porous for oligosaccharides. In a second step, these soluble oligosaccharides
404 formed with linear structure, diffuse into pores (Song 2017). Subsequently, the
405 oligosaccharides can be hydrolyzed to monosaccharides by acid sites (Do Couto Fraga 2016).
406
407 *3.1.5 Temperature-Programmed Desorption of ammonia*
408 Following this line, it is necessary to study the acidity of the synthesized catalysts.
409 Temperature-Programmed Desorption of ammonia (TPD-NH_3) is one of the conventional
410 methods for the characterization of total acidity. In general, the assessment of acidity involves
411 the determination of the strength, number of active centers and their nature. The temperature
412 of desorption can be understood as the relative acidic strength of the different centers. When
413 the strength of the acid centers is higher, the ammonia molecule is retained more strongly
414 and higher temperature is necessary to desorb it. The number of acid centers is defined as the
415 amount of ammonia desorbed per gram of catalyst (Benaliouche 2008).
416 Table 1 shows the quantitative results obtained from the desorption profiles of NH_3,
417 employed to analyze the acidic strength of the m-MOR, calcined Ag/m-MOR and reduced
418 Ag/m-MOR-R catalysts. In the case of mesoporous mordenite support (m-MOR), the
419 baseline is stable after 350°C, indicating that all the ammonia was weakly adsorbed.

However, the calcined and reduced Ag/m-MOR catalysts presented desorption peaks above 350 °C, which indicates the existence of strong acid sites.

Table 1 shows that the total amount of acidic sites increased after incorporating 9.6 wt. % Ag. The maximum temperatures of the desorption peaks are different for the catalysts, which implies a variation in the distribution of the acid strength of the centers after the mesoporosity generation and because of the silver incorporation. The obtained TPD profiles for the m-MOR and Ag/m-MOR samples (not shown), present peaks in two desorption regions: below and above 350 °C. The low temperature peaks correspond to weak acid sites, whereas above 350 °C strong acid sites are detected.

The Ag/m-MOR catalyst shows an increase in the number of strong acid sites of 42 % respect to the original m-MOR mesoporous zeolite. The reduced Ag/m-MOR-R catalyst presented a decrease of the total acid sites respect the calcined sample. In this sense, it is important to notice that in concordance with the NMR results, the chemical composition of the catalysts was changed after the introduction of mesoporosity and silver species.

The mordenite is a zeolite that is characterized by Si (IV) ions forming tetrahedra with the four vertices occupied by O(-II) ions, which are replaced by Al(III) ions. The resulting negative charges are compensated by the presence of metal cations such as K (I) or Na (I), which are introduced extra-framework giving rise to weak Lewis acid centers (Cejka 2010). When the compensation cation is a proton, a Brönsted acid site is generated. The synthesis process to increase the pore size and subsequent introduction of Ag, generated a decrease in the crystallinity of the original zeolite and the presence of extra-reticular octahedral Al. Thus, it is clear that the redox behavior in the mesoporous mordenite is altered by Ag(I) ions.

In the case of the m-MOR support, the synthesis is performed in a basic medium (pH = 11). However, the functionalization with Ag that is carried out at pH = 5 probably promotes the

higher amount of Al(III) ions outside of the crystalline structure. In addition, it is possible that the metal silver particles formed at lower temperatures, improve the dissociation of hydrogen and the reduction of Ag_xO_y species and generation of H^+ sites in strong interaction with the structure are promoted. This implies that the presence of Ag favors the formation of strong acid sites.

3.2 Ultrafast hydrolysis of microcrystalline cellulose

A suspension of microcrystalline cellulose is hydrolyzed in a continuous ultrafast reactor using supercritical water at 400 °C, 25 MPa and 0.03 s of residence time. Under such conditions, more than 99.9 % of cellulose is solubilized and depolymerized into soluble oligomers. Table 2 shows the main composition of the liquid product after SCW treatment of cellulose.

Table 2. Composition of the hydrolysate obtained from cellulose by ultrafast supercritical water hydrolysis (400 °C, 25 MPa, 0.03 s)

	Cellobiose	**Glucose**	**Fructose**	**Glyceraldehyde**	**Glycolaldehyde**	**Oligo-saccharides**	**TOC**
mg·L^{-1}	3159	2697	1348	936	2327	-	10873
%C	12.2	10.0	5.0	3.4	8.6	57.8	-

Total organic carbon in the product was 10873 mg·L^{-1}, being 12.2 % in cellobiose, 10.0 % in glucose, 5% in fructose, 3.4 % in glyceraldehyde and 8.6 % in glycolaldehyde. Pyruvaldehyde concentration is < 3% and neither 5-HMF nor other degradation products such as humins were detected. The oligosaccharides (including cellobiose) represent 70 % in terms of organic carbon, thus, a subsequent hydrolysis step is required to complete their hydrolysis into monomeric sugars.

3.3 Hydrolysis to glucose by heterogeneous catalysts

Table 3 and Figure 5 present the catalytic results of H-MOR, m-MOR and Ag/m-MOR, in N_2 or H_2 atmosphere, in the hydrolysis of the solubilized and partially depolymerized cellulose stream from the supercritical reactor.

The synthesized catalysts were compared with the commercial zeolite in the protonic form (HMOR). Additionally, a blank (no catalyst) test was conducted in hydrogen atmosphere. It was observed that cellobiose and oligosaccharides could be hydrolyzed into glucose at a temperature of 180 °C. The yield to glucose in the blank experiment was 8.9 %, which was considered in the calculation of glucose yield obtained with the catalysts.

No influence of the atmosphere was observed for the HMOR and m-MOR support; the catalytic behavior was similar under inert or reducing atmosphere. The HMOR catalyst showed 55.1 % and 32.8 % of hydrolyzed carbon and D-glucose yield, respectively. However, the sample m-MOR hydrolysed 46.2 % of the carbon present in the feed stream, with a yield of 14.6 % to glucose. In addition, 5- hydroxymethyl furfural (5-HMF) was detected in low concentrations (4.1 - 3.3 %) with both supports.

Table 3. Results of cellulose hydrolysis to D-glucose production

Catalysts	Reaction cond (1)	% C hydrolyzed	$Y_{D\text{-}glucose}$(2)/%	$S_{5\text{-}HMF}$(3)/%
HMOR	H_2	55.1	32.8	4.1
m-MOR	H_2	46.2	14.6	3.3
Ag/m-MOR	H_2	81.8	77.0	4.3
	N_2	77.3	30.3	7.8
Ag/m-MOR-R(4)	H_2	65.1	51.9	10.5
	N_2	63.9	55.8	5.9

(1) Atmosphere of reaction, (2) Yield to D-glucose, %; (3) Yield to 5-HMF, %; (4) Ag/m-MOR-R catalyst reduced in H_2 flow at 500 °C.

After the incorporation of 9.6 wt. % Ag to the m-MOR support, a different catalytic behaviour was observed related to the substrate and the reaction atmosphere. On one hand, when the hydrolysis is carried out in a reducing medium, 81.8 % of the carbon has been

hydrolysed in this catalytic step (Eq. (4)) with a selectivity of 94.1 % to glucose and only a 4.3 % of selectivity to 5-HMF.

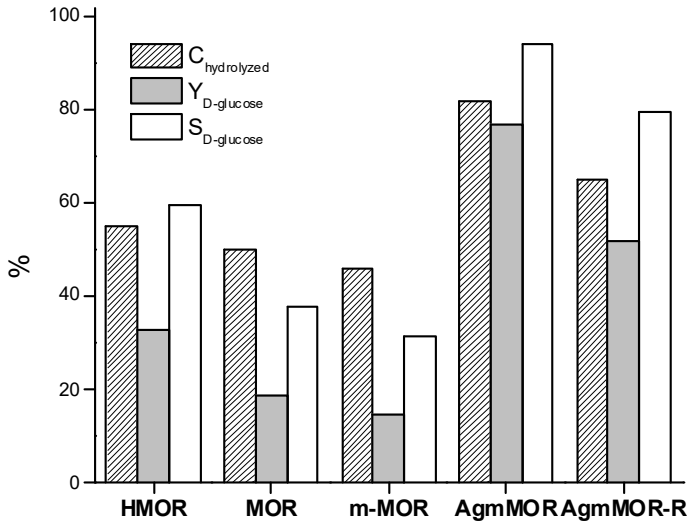

Figure 5. Results of % C hydrolyzed, % D-glucose Yield and % Selectivity to glucose for commercial MOR (Si/Al=6.5), m-MOR, Ag/m-MOR, Ag/m-MOR-R reduced at 500 ºC and H-MOR (Si/Al=10) catalysts for the hydrolysis of cellulose. Reaction conditions: 90 min, 180 ºC, 50 bar H_2 and 1200 rpm

The solubilisation of microcrystalline cellulose in the supercritical water reactor is higher than 99.9 % and after this supercritical step 10.0% of carbon is in glucose form. After the coupling with the subsequent catalytic step using Ag (9.6 wt. %)/m-MOR in a reducing atmosphere, the global glucose yield (including both steps) leads to 63.8 % that is much higher than those obtained in the literature with Ru/CMK-3 (Kobayashi 2010), HY zeolite combined with ionic liquids (Zhang 2009) or a dissolution/precipitation approach in ionic liquids using heterogeneous catalysts with sulfonic groups (Morales-de la Rosa 2018).

In contrast, when the reaction medium is N_2, the amount of hydrolysed oligomers and glucose yield decrease to 77.3 % and 30.3 %, respectively. However, an increase in the production of 5-HMF is detected with a selectivity of 7.8 %.

These results evidence that the reaction atmosphere has a pronounced influence on the hydrolysis reaction. This catalytic performance is directly linked to the Ag species present in the synthesized catalyst. Figure 6 shows a scheme of the proposed hydrolysis mechanisms in the two different reaction media, N_2 (Fig. 6A) and H_2 (Fig. 6B).

Based on the results obtained by TPR (Fig. 2) and XPS (Fig. 3), the calcined Ag/m-MOR catalyst encloses Ag(I) ions located in exchange positions of the mesoporous zeolitic structure and Ag_2O nanoparticles. Since the exchange percentage is 76 %, the catalyst contains a fraction of Na(I) ions not exchanged. When the hydrolysis reaction is carried out in an inert atmosphere (N_2, Fig. 6A), the water occupies the active sites of the catalyst, Ag(I) and Na(I) ions. In previous work, we have studied the interaction between the water molecule and both ions (Aspromonte 2012). The results obtained in this case showed a strong interaction between the water molecule and the exchanged Ag(I) ions. In this way, the water adsorbed on the structure allows the hydrolysis of the oligomers to produce glucose.

In the case where the reaction is carried out in reducing medium (H_2, Fig. 6B), an additional effect is produced. At 180 °C, the fraction (almost complete) of Ag_2O nanoparticles supported on the catalyst is reduced, to generate metal silver particles and water (Fig. 6-B1), thus shifting the reaction towards glucose (Westermann 2012).

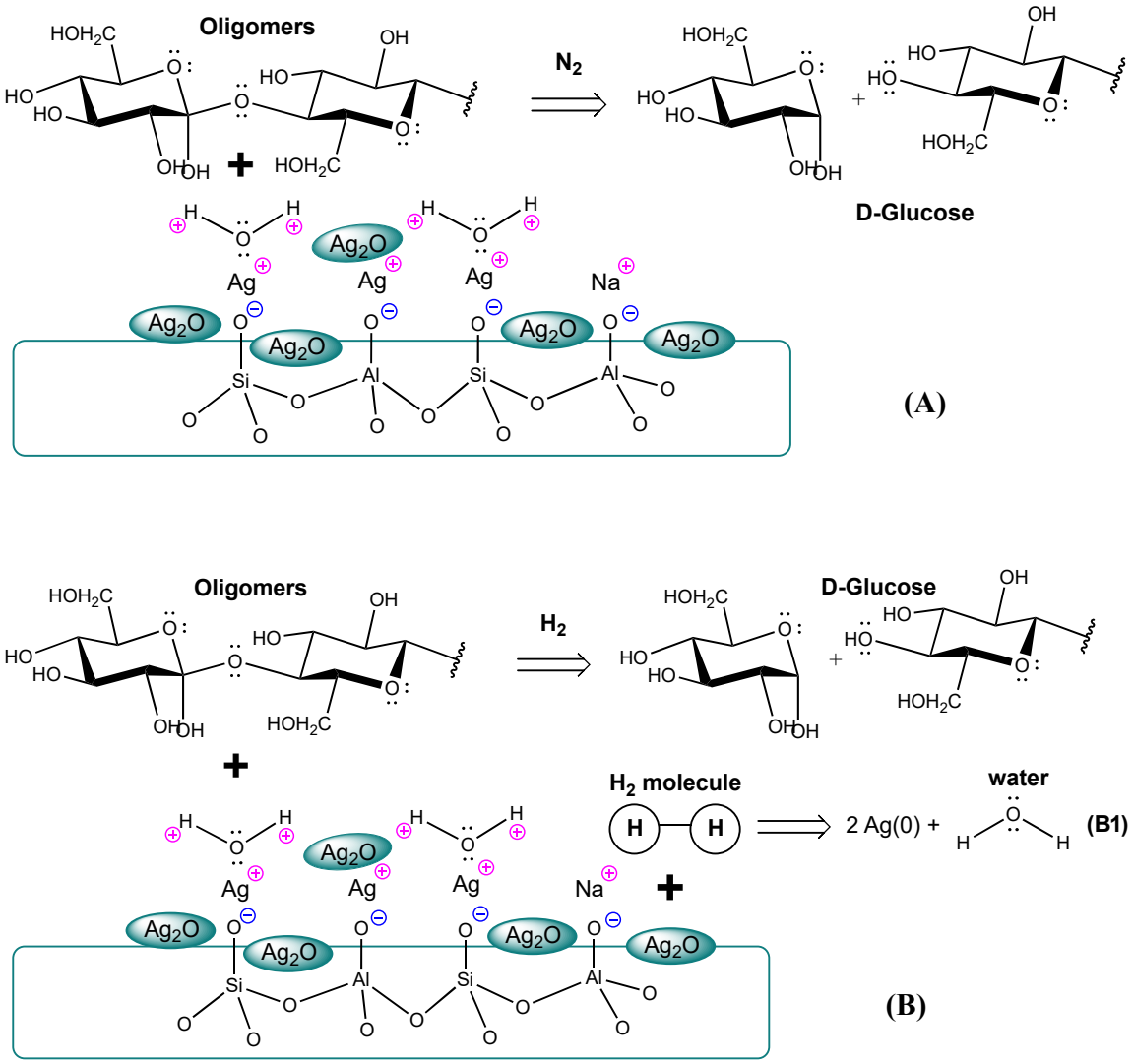

Figure 6. Scheme of the pathway proposed for the hydrolysis of oligomers to produce glucose over silver-mesoporous zeolite catalysts, (A) in N_2 atmosphere and (B) in H_2 atmosphere.

Thus, in order to study this, the calcined Ag/m-MOR catalyst was previously reduced at 500 °C (called Ag/m-MOR-R) and it was evaluated in nitrogen or hydrogen atmosphere. In this sense, it was observed that the amount of hydrolyzed carbon is the same in both reaction atmospheres. However, in the presence of hydrogen it is observed that production of glucose decreases to 51.9% and the selectivity to 5-HMF increases (10.5 %). In all cases it is observed that the glucose selectivity decreases due to the increase in the production of the degradation

573 compound 5-HMF. This result corroborates the mechanism proposed in Fig. 6, because by
574 reducing the catalyst at 500 ºC prior to the reaction, the supported Ag_2O nanoparticles were
575 reduced as well as the majority fraction of Ag(I) ions exchanged in the structure. This implies
576 that the catalytic performance of the sample Ag/m-MOR-R decreases in comparison with the
577 calcined sample and it does not depend of the used reaction medium, because the reduction
578 of Ag_2O does not occur.
579 Therefore, it is important to notice that using heterogeneous Ag catalysts exchanged in
580 mesoporous zeolitic structures, a glucose yield of 77 % was obtained with a selectivity of
581 94.1 % at 180 °C for 90 minutes. In the literature, a glucose yield of 50.5% and selectivity of
582 90% are reported with the homogeneous heteropoly acid $H_3PW_{12}O_{40}$ at 180 ºC and 2 h (Tian
583 2010). Similarly, acidified mesoporous carbons of the CMK-3-SO_3H type, operating for 24
584 hours at 150 °C, produce 74.5 % of glucose yields (Pang 2010). Zeolites such as H-beta and
585 HY hydrolyzing for 24 h at 150 °C or 2 h at 130 °C allow to obtain glucose yields of 12 and
586 50%, respectively (Cai 2012). Consequently, the yield and glucose selectivity values
587 obtained in the present work, with recoverable heterogeneous catalysts, greatly exceed what
588 is reported in the open literature.
589
590 **3.4 Recycling test and carbon deposits**
591 The catalytic stability of the solid Ag/m-MOR was evaluated in 5 consecutive hydrolysis
592 cycles. The activity of the catalyst after each cycle was expressed in terms of % C hydrolyzed
593 (Eq. 4), glucose yield (Eq. 3) and selectivity towards glucose (Eq. 1) and 5-HMF (Eq. 5). The
594 obtained results are shown in Figure 7.
595 A deactivation of the catalyst between the first and the third reaction cycle is observed, which
596 is manifested by the reduction of the hydrolyzed carbon up to 45.6 % and the glucose yield

to 37.3%. It is important to notice that, although the catalysts exhibit an expected decrease in the amount of hydrolyzed carbon and in the glucose yield, the selectivity towards glucose remains practically constant, with values varying between 91.7 and 81.8 %. After the third reaction cycle, the values of the parameters that are linked to the catalytic activity remain practically constant until the fifth reaction cycle. The yield to glucose is in the range 37.3-38.8 % and the amount of hydrolyzed carbon between 45.6-47.1 %.

There are not many works in the literature that report activities of catalysts in the hydrolysis of cellulose after various reaction cycles. Suganuma et al. (Suganuma 2008), reported that the activity of an amorphous carbon bearing SO_3H, -COOH, -OH functions do not decrease after 25 reuses (total reaction time, 150 h), however, the observed glucose yield was only 4 %. Fang et al. and Zhang et al. (2011) prepared hydrotalcite nanoparticles ($Mg_4Al_2(OH)_{12}CO_3$) for the hydrolysis of cellulose and they show a maximum glucose yield of 30.8 % at 150 ºC after 24 h that can be reused four times without much drop in the catalytic activity. In any case, the works in open literature reported recycling tests corresponding to maximum glucose yields much lower than that of the present work.

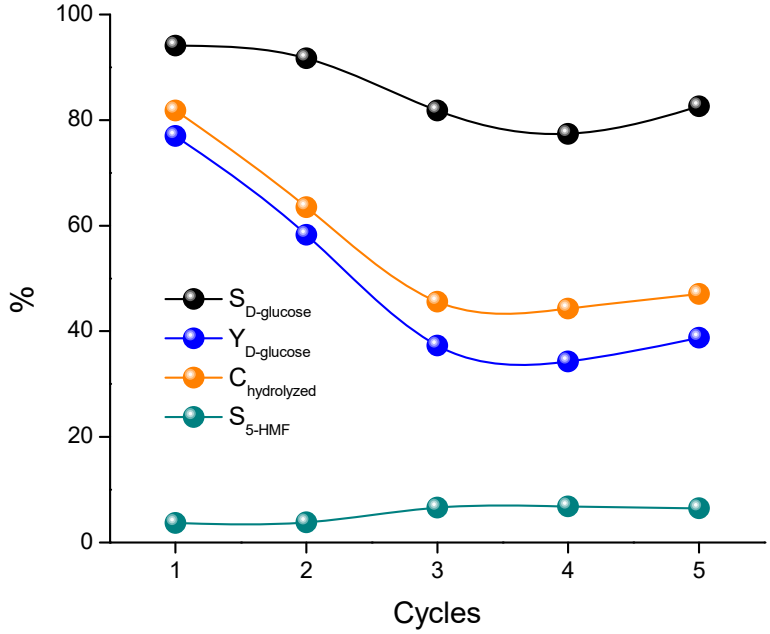

Figure 7. Results of (a) % Selectivity to glucose, (b) % C hydrolyzed, (c) % D-glucose Yield and (d) % Selectivity to HMF for Ag/m-MOR catalyst after 5 cycles of oligomers hydrolysis. Reaction conditions for each cycle: 90 min, 180 ºC, 50 bar H_2 and 1200 rpm.

To understand this behaviour, it is important to note that the reasons for deactivation could be classified in two groups, which directly modify active sites such as sintering or metal loss and those responsible for blocking the catalyst such as coke formation. To study the formation of coke during the successive cycles of catalytic reaction, temperature-programmed oxidation (TPO) measurements were carried out. The TPO profiles of the deactivated catalyst show a peak with a maximum ranging between 390 and 420 ºC, attributed to an amorphous coke that encapsulates the active sites. Table 4 presents the results derived from TPO analysis after each reaction cycle.

Table 4. Diameter of silver metallic particles and carbon characterization deposited on Ag/m-MOR catalysts after 5 reaction cycles. Reaction conditions: 180 ºC, 90 min, 0.06 g metal/g carbon.

Cycles	wt. % carbon	T_{max} / ºC	$D_{Ag(0)}$/nm[a]
1st	0.07	400	17.5
2nd	0.10	420	23.6
3rd	0.15	390	32.3
4th	0.17	410	36.6
5th	0.18	400	37.1

[a] Diameter of silver metallic particle (nm) calculated by Scherrer equation: $D_{Ag(0)} = k\lambda/(\beta \cos\theta)$, where λ is the X-ray source wavelength (1.5406 Å), β is the angular width ~FWHM and θ is the half angle of diffraction.

The amount of coke increases twice after the third reaction cycle and remains practically constant until the fifth reaction cycle.

On the other hand, Figure 8 shows the XRD results in the range of 2θ = 30 - 85 grades after each reaction cycle, to analyze the modification of active sites. All the diffractograms present

four peaks at 2θ = 38.1º, 44.3º, 64.4º and 77.4º, corresponding to Ag(0) particles (Ausavasukhi 2008). The average size of the metallic silver particles was reported in Table 4 and it was calculated using the Scherrer equation (Sales 1998).

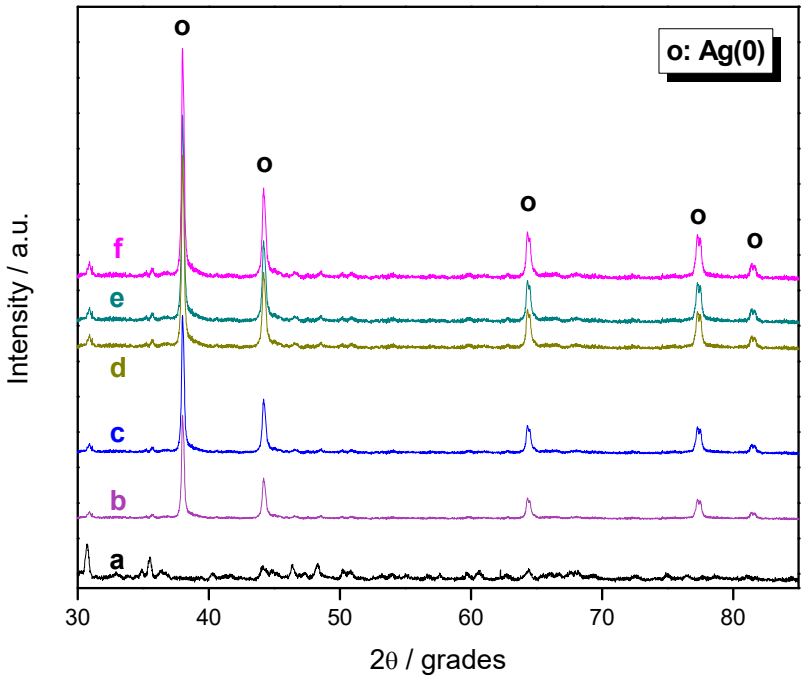

Figure 8. XRD results obtained for (a) calcined Ag/m-MOR catalyst and (b-f) after used (1-5) cycles in hydrolysis reaction: 90 min, 180 ºC, 50 bar H_2 and 1200 rpm.

The average diameter of the Ag(0) crystallite generated during the hydrolysis reaction ranges from 17.5 to 37.1 nm. A more pronounced increase in the average crystal size is observed in the third reaction cycle, which agrees with the observed catalytic deactivation. In this sense, considering that the estimated pore diameter presented in Table 1 is between 3.9 and 4.1 nm, the presence of Ag (0) particles together with the formation of coke are responsible for the partial blockage of the pores of the mesoporous zeolite support and therefore the loss of catalytic activity.

4. Conclusions

The combination of supercritical water hydrolysis of cellulose in ultrafast reactors with the subsequent hydrolysis of the cello-oligosaccharides on Ag/m-MOR catalyst has led to a glucose yield of 77.0 % and a percentage of hydrolyzed carbon in the catalytic step of 81.8 %.

The chemical composition of the catalysts changed after introducing mesoporosity and silver species. The presence of Ag (I) ions in strong interaction with the mesoporous zeolitic structure was observed. Thus, a rearrangement of the acidic sites was detected producing ammonia desorption peaks at temperatures above 350 °C in the TPD-NH_3 analysis. This infers the production of strong acid sites as a consequence of ion exchange in acid medium. NMR and XPS detected the presence of octahedral Al (III) species that could be responsible for the high catalytic activity in terms of conversion of the carbon and yield to glucose.

A deactivation of the catalyst between the first and the third reaction cycle is observed, after which, the activity remains constant up to fifth cycle. The hydrolyzed carbon diminishes up to 45.6% and the D-glucose yield to 37.3%, although the selectivity to glucose remains relatively constant at values between 91.7 and 81.8%. The presence of Ag(0) particles together with the formation of coke are responsible for the partial blockage of the pores of the mesoporous zeolite support and the loss of catalytic activity.

Acknowledgements

This work was supported by Spanish Government through the Research Project CTQ2015-64892-R (MINECO/FEDER) and ANPCyT (PICT 2014-2445) and CONICET (PIP 11220090100190, PIP 11220130100062). The authors also acknowledge the financial

708 support received from UNL. They are grateful to ANPCyT for the purchase of the SPECS
709 multi-technique analysis instrument (PME8-2003). Thanks are given to Fernanda Mori and
710 Magali Borne for the XPS and NMR measurements, respectively.

References

Abdelrasoul A, Zhang H, Cheng CH, Doan H (2017) Applications of molecular simulations for separations and adsorption in zeolites. Microp Mesop Mater 242:294-348

Amama PB, Pint CL, Kim SM, McJilton L, Eyinc KG, Stach EA, Hauge RH, Maruyama B (2010) Influence of alumina type on the evolution and activity of alumina-supported Fe catalysts in single-walled carbón nanotube carpet growth. ACS Nano 4:895-904

Aspromonte SG, Miró EE, Boix AV (2012) Effecy of Ag-Co interactions in the mordenite on the NO_x SCR with butane and toluene. Catal Comm 28:105-110

Aspromonte SG, Mizrahi MD, Alonso E, Ramallo-López JM, Boix AV (2017) Co/MCM41 catalyst in the COProx reaction prepared by supercritical CO_2 reactive deposition. Microp Mesop Mater 239:147-157

Aspromonte SG, Mizrahi MD, Schneeberger FA, Ramallo-López JM, Boix AV (2013) Study of the nature and location of silver in Ag-exchanged mordenite catalysts. Characterization by spectroscopic techniques. J Phys Chem C 117:25433-25442

Aspromonte SG, Miró EE, Boix AV (2012) FTIR studies of butane, toluene and nitric oxide adsorption on Ag exchanged NaMordenite. Adsorption 18:1-12

Ausavasukhi A, Suwannaran S, Limtrakul J, Sooknoi T (2008) Reversible interconversion behavior of Ag species in AgHZSM-5:XRD, ^{1}H MAS NMR, TPR, TPHE, and catalytic studies. Appl Catal A: Gen 345: 89-96

Benaliouche F, Boucheffa Y, Ayrault P, Mignard S (2008) NH_3-TPD and FTIR spectroscopy of pyridine adsorption studies for characterization of Ag- and Cu-exchanged X zeolites. Microp Mesop Mater 111:80-88

Boix AV, Miró EE, Lombardo EA, Fierro JLG (2008) The inhibiting effect of extra-framework Al on monolithic Co-ZSM5 catalysts used for NOx SCR. Catal Today 133-135:428-434

Brunauer S, Emmett PH, Teller E (1938) Adsorption of gases in multimolecular layers. JACS 60:309-319

Cai HL, Li CZ, Wang AQ, Xu GL, Zhang T (2012) Zeolite-promoted hydrolysis of cellulose in ionic liquid, insight into the mutual behavior of zeolite, cellulose and ionic liquid. Appl. Catal B: Environ 123–124: 333–338

Cantero D, Bermejo M, Cocero M (2013) High glucose selectivity in pressurized water hydrolysis of cellulose using ultra-fasr reactor. Biores Tech 135:697-703

Cantero DA, Sánchez Tapia Á, Bermejo MD (2015) Pressure and temperatura effect on cellulose hydrolysos in pressurized water. Chem Eng J 276:145-154

Cantero DA, Vaquerizo L, Mato F, Bermejo MD, Cocero MJ (2015) Energetic approach of biomass hydrolysis in supercritical water. Biores Tech 179:136-143

Cejka J, Corma A, Zones S (2010) Zeolites and catalysis: synthesis, reactions and applications. Wiley-VCH, Germany

749 Chheda JN, Huber GW, Dumesic JA (2007) Liquid-phase catalytic processing of biomass-
750 derived oxygenated hydrocarbons to fuels and chemicals. Angew Chem Int Ed 46:7164-7183

751 Chimentao RJ, Lorente E, Gispert-Guirado F, Medina F, López F (2014) Hydrolysis of dilute
752 acid-pretreated cellulose under mild hydrothermal conditions. Carbohydr Polym 111:116-
753 124

754 Cho HJ, Dornath P, Fan W (2014) Synthesis of hierarchical Sn-MFI as Lewis acid catalysts
755 for isomerization of cellulosic sugars. ACS Catal 4:2029-2037

756 Claus P, Hofmeister H (1999) Electron microscopy and catalytic study of silver catalysts:
757 structure sensitivity of the hydrogenation of crotonaldehyde. J Phys Chem B 103:2766-2775

758 do Couto Fraga A, Bittencourt Quitete CP, Ximenes VL, Falabella Sousa-Aguiar E, Botelho
759 Rego M (2016) Biomass derived solid acids as effective hydrolysis catalysts. J Mol Catal A:
760 Chem 422:248-257

761 Fang Z, Zhang F, Zeng HY, Guo F (2011) Production of glucose by hydrolysis of cellulose
762 at 423 K in the presence of activated hydrotalcite nanoparticles. Bioresour Technol 102:
763 8017–8021

764 Gardner DW, Huo J, Hoff TC, Johnson RL, Shanks BH, Tessonnier JP (2015) Insights into
765 the hydrothermal stability of ZSM-5 under relevant biomass conversion reaction conditions.
766 ACS Catal 5:4418-4422

767 Hu L, Lin L, Wu Z, Zhou S, Liu S (2015) Chemocatalytic hydrolysis of cellulose into glucose
768 over solid acid catalysts. Appl Catal B: Environ 174-175:225-243

769 Inumaru K, Ishihara T, Kamiya Y, Okuhara T, Yamanaka S (2007) Water-tolerant, highly
770 active solid acid catalysts composed of the kegging-type polyoxometalate $H_3PW_{12}O_{40}$
771 immobilized in hydrophobic nanospaces of organomodified mesoporous silica. Angew Chem
772 Int Ed 46:7625-7628

773 Kobayashi H, Komanoya T, Hara K, Fukuoka A (2010) Water-tolerant mesoporous-carbon-
774 supported ruthenium catalysts for the hydrolysis of cellulose to glucose. ChemSusChem
775 3:440-443

776 Meynen V, Cool P, Vansant EF (2009) Verified syntheses of mesoporous materials. Microp
777 Mesop Mater 125:170-223

778 Mignoni ML, Petkowicz DI, Fernandez Machado NRC, Pergher SBC (2008) Synthesis of
779 mordenite using kaolin as Si and Al source. Appl Clay Sc 41:99–104

780 Morales-delaRosa S, Campos-Martin JM, Fierro JLG (2018) Chemical hydrolysis of
781 cellulose into fermentable sugars through ionic liquids and antisolvent pretreatments using
782 heterogeneous catalysts. Catal Today 302:87-93

783 Pang J, Wang A, Zheng M, Zhang T (2010) Hydrolysis of cellulose into glucose over carbons
784 sulfonated at elevated temperatures. Chem Comm 46:6935-6937

785 Ravenelle RM, Diallo FZ, Crittenden JC, Sievers C (2012) Effects of metal precursors on the
786 stability and observed reactivity of $Pt/\gamma\text{-}Al_2O_3$ catalysts in aqueous phase reactions. Chem
787 Cat Chem 4:492-494

Saha B, Abu-Omar MM (2014) Advances in 5-hydroxymethylfurfural production from biomass in biphasic solvents. Green Chem 16:24-38

Sales EA, Benhamida B, Caizergues V, Lagier J-P, Fiévet F, Bozon-Verduraz F (1998) Alumina-supported Pd, Ag and Pd-Ag catalysts: Preparation through the polyol process, characterization and reactivity in hexa-1,5-diene hydrogentation. Appl Catal A: Gen 172: 273-283

Song S, Di L, Wu G, Dai W, Guan N, Li L (2017) Meso-Zr-Al-beta zeolite as a robust catalyst for cascade reactions in biomass valorization, Appl Catal B: Env 205:393-403

Stepanov AG (2016) Basics of Solid-State NMR for Application in Zeolite Science. In: Sels B, Kustov L (ed) Zeolites and Zeolite-like Materials, 1st edn. Elsevier, Netherlands, pp 137-188

Suganuma S, Nakajima K, Kitano M, Yagamuchi D, Kato H, Hayashi S, Hara M (2008) Hydrolysis of cellulose by amorphous carbon bearing SO_3H, COOH, and OH groups. J Am Chem Soc 130:12787-12793

Tian J, Wang J, Zhao S, Jiang C, Zhang X, Wang X (2010) Hydrolysis of cellulose by the heteropoly acid $H_3PW_{12}O_{40}$. Cellulose 17:587-594

Waterhouse GIN, Metson JB, Bowmaker GA (2007) Synthesis, vibrational spectra and thermal stability of Ag_3O_4 and related Ag_7O_8X salts. Polyhedron 26:3310-3322

Westermann A, Azambre B, Koch A (2012) Effect of Ag, Pd and Co promoters on the Selective Catalytic Reduction (SCR) of NOx by ethanol over sulfated ceria-zirconia catalysts. Catal Today 19:65-74

Yamaguchi D, Kitano M, Suganuma S, Nakajima K, Kato H, Hara M (2009) Hydrolysis of cellulose by a solid acid catalyst under optimal reaction conditions. J Phys Chem C 113:3181-3188

Zhang Z, Zhao ZK (2009) Solid acid and microwave-assisted hydrolysis of cellulose in ionic liquid. Carbohydr Res 344:2069-2072